A Framework to Assess the Influence of Different Cardiac Fibrosis Phenotypes and Border Zone on Arrhythmogenesis

Guilherme M. Couto[1], **Joventido O. Campos**[1,2], **Rodrigo W. dos Santos**[1,2]

[1]Graduate Program in Computational Modeling, Federal University of Juiz de Fora, Juiz de Fora, Minas Gerais, Brazil

[2]Department of Computer Science, Federal University of Juiz de Fora, Juiz de Fora, Minas Gerais, Brazil

Abstract. *Current computational models often oversimplify cardiac fibrosis, lacking micro-architecture details. To address this, we present a scalable computational pipeline extending a histologically-calibrated Perlin noise generator to automatically construct focal fibrotic cores and functional border zones. Using this framework, we conducted preliminary 2D electrophysiological simulations under localized hypoxia to evaluate four distinct phenotypes. Initial results suggest that phenotype influences tissue vulnerability, with diffuse architectures exhibiting a higher incidence of reentries under the tested conditions. Furthermore, the framework successfully models geometrically constrained lesions, highlighting that variations in the total diseased area between global and focal models substantially alter the number of arrhythmic events. This work underscores the importance of incorporating spatial heterogeneity and appropriate boundary constraints in predictive computational modeling.*

1. Introduction

Following cardiac injury, excessive extracellular matrix (ECM) accumulation creates diverse fibrotic patterns that disrupt electrical continuity [De Jong et al. 2011]. These structural heterogeneities, combined with localized hypoxia, alter cardiomyocyte electrophysiology and provide a potential substrate for reentrant circuits and sustained arrhythmias [Oliveira et al. 2018, Sachetto et al. 2018, Shaw and Rudy 1997].

Computational modeling is indispensable to dissect these mechanisms [Sachetto et al. 2018, Oliveira et al. 2018]. However, current clinical imaging lacks the spatial resolution to capture micro-architectural details [Ravassa et al. 2023]. Consequently, *in silico* studies often rely on oversimplified geometric shapes or uniform distributions that lack biological fidelity.

To address this, Lawson et al. developed a histologically calibrated Perlin noise generator to reproduce cardiac fibrosis phenotypes [Lawson et al. 2024]. These patterns include *compact* (dense, contiguous blocks), *diffuse* (short, scattered strands), *interstitial* (reticular mesh separating fibers), and *patchy* fibrosis (irregular clusters with elongated strands) [De Jong et al. 2011], as shown in Fig. 1. Although powerful to reproduce histological slices, the original generator inherently lacks the spatial decoupling necessary to model focal lesions with a functional border zone, a transitional region where decaying collagen and metabolic gradients critically modulate wavefront dynamics.

In this work, we propose a scalable framework that extends the Lawson et al. generator [Lawson et al. 2024] to construct heterogeneous simulation domains. We hy-

pothesize that specific morphological phenotypes may differentially impact arrhythmia probability and that this behavior is modulated by spatial constraints. Preliminary 2D simulations evaluate these architectures, suggesting that each phenotype presents a distinct risk profile. Crucially, we demonstrate the framework's capability to model geometrically constrained lesions with transition zones, highlighting how spatial restrictions and differences in total fibrotic area alter the absolute number of arrhythmic events compared to fully diseased domains.

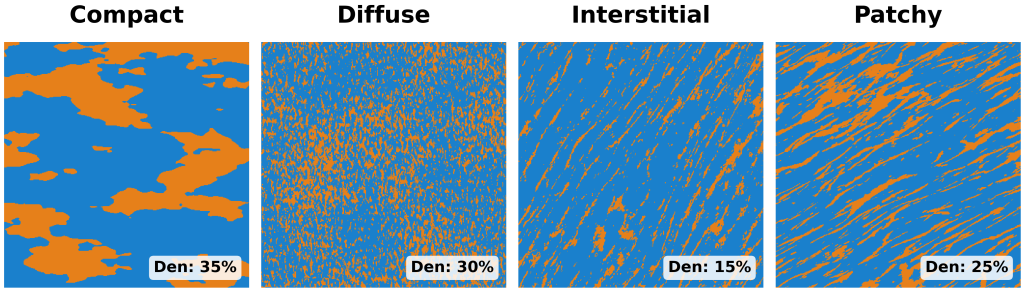

Figure 1. Generated samples of the four fibrosis phenotypes.

2. Architecture and Implementation

To effectively simulate focal lesions, it is necessary to decouple the spatial location of the scar from the textural generation of the collagenous network. This separation allows for the creation of complex, multi-regional domains. By utilizing the foundational multi-octave Perlin noise engine from Lawson et al. [Lawson et al. 2024], we abstracted the pattern generation into a three-stage computational pipeline: spatial definition, texture generation, and adaptive thresholding. Figure 2 shows an overview of this process.

2.1. Spatial Definition and Resolution

The first stage constructs the physical layout of the simulation domain using binary masks to define regions such as the Fibrotic Core (FC) and the surrounding healthy myocardium. To represent the transition, a functional Border Zone (BZ) is efficiently computed by applying a distance transform to the FC mask, instantly defining gradient layers.

It is important to acknowledge that the simulations in this preliminary study utilize a spatial discretization of 100 μm. While this resolution is relatively coarse for capturing true micro-anatomical structures and may underestimate conduction blocks compared to advanced homogenization techniques, it is sufficient to preserve the macroscopic structural archetypes of each phenotype for our comparative structural analysis.

2.2. Texture Generation

Once the spatial regions are defined, the pipeline computes a continuous, multi-octave Perlin noise field over the entire domain. The specific parameters governing the base noise topology, density variation fields, and anisotropic fiber selection are maintained from the original model. This guarantees that the underlying algorithm preserves the structural signatures of the four distinct phenotypes, even when applied to novel geometries.

2.3. Adaptive Thresholding

The final stage merges the spatial definitions with the noise field to produce the binary mesh, distinguishing conductive myocytes from the non-conductive fibrosis. To ensure quantitative consistency, a bisection method is employed to dynamically determine the exact threshold value required to match the target fibrosis density strictly within the FC.

To model the transitional environment of the BZ, a spatially varying gradient is applied to this threshold. Specifically, the threshold value is linearly increased from the edge of the core toward the healthy tissue. It must be noted that, due to the inherent value distribution of Perlin noise, applying a linear increase to the threshold does not guarantee a linear decay in the probability of collagen deposition. Nevertheless, this approach effectively generates a decaying transitional structure. In this preliminary phase, other mathematical forms of spatial gradients for the BZ were not evaluated.

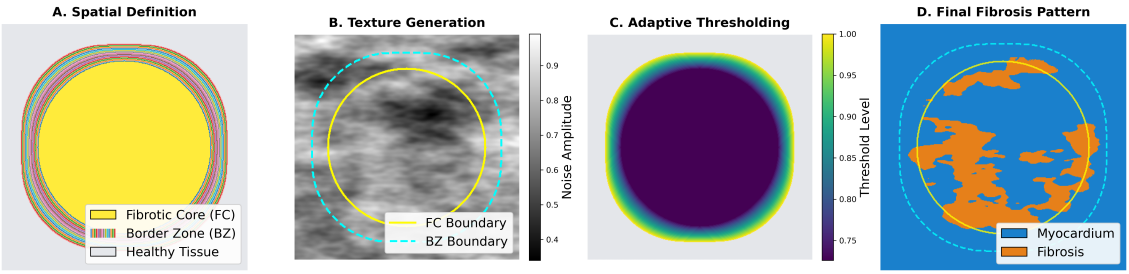

Figure 2. The framework operates in distinct stages: (A) The geometric boundaries of FC and the BZ layers. (B) The multi-octave Perlin noise field. (C) The spatial gradient with the calculated threshold values. (D) The final binary pattern with fibrosis and myocardium.

3. Experimental Setup and Simulation Scenarios

To evaluate the arrhythmogenic impact of the spatially constrained fibrosis patterns, we conducted high-performance electrophysiological simulations using MonoAlg3D, an open-source solver optimized for parallel GPU execution [Sachetto Oliveira et al. 2018].

Human ventricular electrophysiology was simulated using the ten Tusscher model (TT3) [Ten Tusscher and Panfilov 2006]. To physiologically represent the entrapped cardiomyocytes within the fibrotic core, the standard equations were adapted to account for intracellular ATP depletion [Sachetto et al. 2018], simulating the local hypoxic stress commonly found in diseased tissue. The tissue was modeled using the standard monodomain reaction-diffusion equation on a regular grid with a spatial resolution of 100 μm and a fixed temporal discretization step of 0.02 ms.

To account for the stochastic nature of the generator and ensure statistical robustness, we performed a comprehensive parameter sweep. For each of the four phenotypes, the target collagen density was varied from 5% to 90% in 5% increments. An ensemble of 400 distinct microstructural samples was generated for every unique combination by permuting 100 random seeds across four fiber orientations (0°, 30°, 60°, and 90°).

Using these generated meshes, we evaluated two distinct two-dimensional configurations, each measuring 4×4 cm: **Scenario I (Global Fibrosis)**: The entire simulation

domain was subjected to the specific fibrosis pattern and uniform acute hypoxia; **Scenario II (Focal Lesion)**: The fibrotic substrate was spatially confined to a central circular core (2.8 cm diameter), surrounded by healthy myocardium. A border zone (10% of the core's diameter) was generated around the core. Within this transitional layer, both the metabolic hypoxic stress and the probability of collagen deposition decayed linearly to interface smoothly with the healthy tissue.

For both scenarios, a standard planar stimulus was applied to the left side of the domain, and the outcome was classified as a sustained arrhythmia if continuous electrical activation persisted for more than 1000 ms.

4. Preliminary Results and Discussion

To demonstrate the capabilities of the proposed spatial framework and assess the structural impact of different fibrosis morphologies, we analyzed the number of sustained arrhythmias generated across the simulations, as well as the underlying wavefront dynamics.

In Scenario I, where the entire 16 cm^2 domain was uniformly subjected to fibrosis, a hierarchy of severity emerged based on the micro-architectural phenotype (Figure 3). The structural archetypes dictated distinct interactions with the propagating wavefront. *Diffuse* fibrosis acted as the most vulnerable substrate, exhibiting the highest absolute number of sustained reentries (333 events). Its highly scattered nature severely fractionates the wavefront, generating multiple anchor points that sustain complex micro-reentries. *Interstitial* and *patchy* architectures presented intermediate arrhythmogenic profiles (yielding 226 and 121 events, respectively); these patterns force the electrical signal to navigate through tortuous, zig-zag conduction pathways, which also promotes wave break. Conversely, *compact* fibrosis resulted in only 4 sustained reentries. Its dense and contiguous blocks typically provide a single anchor point, forcing the wavefront to travel around the obstacle in much longer reentry circuits that are more likely to self-terminate or collide with domain boundaries.

Crucially, evaluating the focal lesion generated by our pipeline (Scenario II) allowed us to observe the interaction between the FC, the BZ, and the healthy myocardium. Clinical and experimental literature points to the BZ as a primary arrhythmogenic risk factor [Oliveira et al. 2018]. In our simulations, the spatial behavior of the arrhythmias varied significantly by phenotype. For the *diffuse*, *interstitial*, and *patchy* phenotypes, the reentrant circuits predominantly initiated and anchored within the FC, subsequently spreading outward through the BZ into the healthy domain. In contrast, for the *compact* phenotype, the reentrant circuits were more expansive, dynamically involving the physical obstacle of the FC, the transitional BZ, and the surrounding healthy tissue to sustain their longer continuous pathways.

As illustrated in Figure 3, the introduction of these geometric constraints resulted in a substantial reduction in the total number of sustained events across all active phenotypes. For instance, the incidence in the *diffuse* phenotype dropped from 333 events in the global scenario to 123 events in the focal configuration. However, this attenuation must be interpreted cautiously. While the global scenario presented 16 cm^2 of fibrotic substrate, the focal lesion comprised approximately 9 cm^2 (including the BZ). Therefore, the reduced absolute number of reentrant events primarily reflects this significant disparity in the available substrate for wavefront fractionation, rather than indicating that

the framework's BZ inherently prevents arrhythmias. It is also interesting to notice that, despite the overall reduction, the incidence hierarchy remains the same. These preliminary findings highlight the flexibility of the proposed pipeline in modeling geometrically constrained lesions and emphasize how spatial restrictions profoundly alter the baseline structural vulnerability compared to fully diseased models.

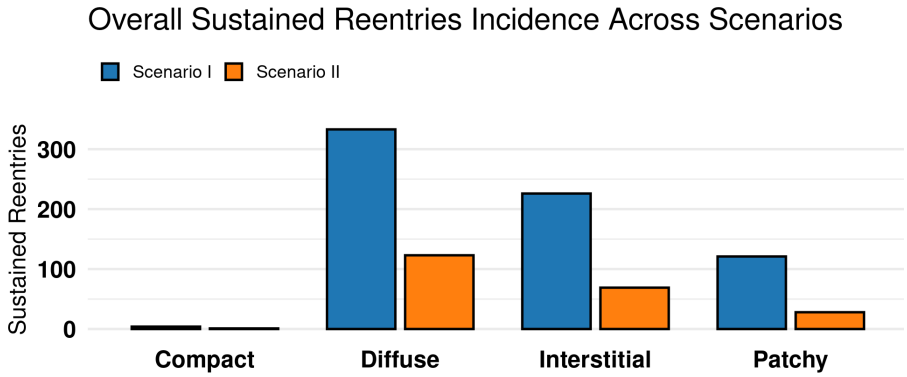

Figure 3. Total number of sustained reentries by fibrosis pattern. Bars represent the absolute count of arrhythmic events across all simulations between the Scenario I (blue) and the Scenario II (orange) for each phenotype.

5. Conclusion

In this work, we presented a scalable computational pipeline that expands a Perlin noise generator to model spatially heterogeneous cardiac fibrosis. By decoupling the lesion's spatial definition from its textural generation via distance transforms and adaptive thresholding, the framework constructs FCs and functional BZs.

Preliminary electrophysiological simulations suggest that tissue vulnerability is strongly influenced by the micro-architectural phenotype. *Diffuse* promotes severe wavefront fractionation and acts as the most vulnerable substrate for reentrant circuits under the tested conditions. Conversely, *compact* typically provides single anchor points that favor wave termination. Furthermore, our results highlight the framework's capability to accurately model geometrically constrained lesions.

As an initial study, several limitations must be acknowledged. The analysis is restricted to 2D idealized slabs, neglecting the conduction pathways present in the volumetric myocardium. Structurally, the 100 μm spatial discretization successfully preserves macroscopic structural archetypes but remains a coarse approximation for true micro-anatomical structures. Additionally, the arrhythmogenic contributions of the fibrosis were not isolated from hypoxia, and alternative mathematical gradients for BZ thresholding have yet to be evaluated.

Future work will prioritize isolated analyses to evaluate structural and ionic drivers independently. We also aim to apply inferential statistical modeling to quantify non-linear risk shifts across fibrosis densities. Ultimately, we plan to deploy this automated pipeline in 3D environments. Given its scalable and geometry-agnostic nature, the framework holds significant potential for direct integration with segmented clinical masks derived from Cardiovascular Magnetic Resonance, allowing the incorporation of appropriate structural archetypes into personalized clinical risk assessments.

6. Declaration of Generative AI Use

During the preparation of this work, Artificial Intelligence was employed to aid in the generation of data analysis plots, support the organization and refactoring of the underlying codebase, and assist with English translation, grammar correction, and overall text refinement. All AI-assisted outputs were rigorously reviewed, validated, and edited by the authors, who assume full responsibility for the final content, integrity, and original ideas presented in this manuscript.

7. Acknowledgments

The authors acknowledge support from the Wellcome Trust (214290/Z/18/Z), EPSRC via the CompBioMedX project (EP/X019446/1), CompBioMed2 (GA 675451, 823712), FAPEMIG (APQ-02752-24; APQ-02445-24; APQ-02513-22), FINEP (SOS Equipamentos AV020062/22), SINAPAD Santos-Dumont, CNPq, CAPES, EBSERH, and UFJF.

References

De Jong, S., van Veen, T. A., van Rijen, H. V., and de Bakker, J. M. (2011). Fibrosis and cardiac arrhythmias. *Journal of cardiovascular pharmacology*, 57(6):630–638.

Lawson, B. A., Drovandi, C., Burrage, P., Bueno-Orovio, A., Dos Santos, R. W., Rodriguez, B., Mengersen, K., and Burrage, K. (2024). Perlin noise generation of physiologically realistic cardiac fibrosis. *Medical Image Analysis*, 98:103240.

Oliveira, R. S., Alonso, S., Campos, F. O., Rocha, B. M., Fernandes, J. F., Kuehne, T., and Dos Santos, R. W. (2018). Ectopic beats arise from micro-reentries near infarct regions in simulations of a patient-specific heart model. *Scientific reports*, 8(1):16392.

Ravassa, S., Lopez, B., Treibel, T. A., San Jose, G., Losada-Fuentenebro, B., Tapia, L., Bayes-Genis, A., Diez, J., and Gonzalez, A. (2023). Cardiac fibrosis in heart failure: Focus on non-invasive diagnosis and emerging therapeutic strategies. *Molecular aspects of medicine*, 93:101194.

Sachetto, R., Alonso, S., and Dos Santos, R. W. (2018). Killing many birds with two stones: hypoxia and fibrosis can generate ectopic beats in a human ventricular model. *Frontiers in Physiology*, 9:764.

Sachetto Oliveira, R., Martins Rocha, B., Burgarelli, D., Meira Jr, W., Constantinides, C., and Weber dos Santos, R. (2018). Performance evaluation of gpu parallelization, space-time adaptive algorithms, and their combination for simulating cardiac electrophysiology. *International journal for numerical methods in biomedical engineering*, 34(2):e2913.

Shaw, R. M. and Rudy, Y. (1997). Electrophysiologic effects of acute myocardial ischemia: a mechanistic investigation of action potential conduction and conduction failure. *Circulation research*, 80(1):124–138.

Ten Tusscher, K. H. and Panfilov, A. V. (2006). Alternans and spiral breakup in a human ventricular tissue model. *American Journal of Physiology-Heart and Circulatory Physiology*, 291(3):H1088–H1100.